Spitzer observations of the thermal emission from WASP-43b: the closest hot Jupiter around a cool K star

Jasmina Blecic[1], Joseph Harrington[1], Nikku Madhusudhan[2], Kevin B. Stevenson[1], Ryan A. Hardy[1], Patricio Cubillos[1], Sarah Nymeyer[1], David R. Anderson[4], Coel Hellier[4], Andrew Collier Cameron[4], Alexis M. S. Smith[3]

[1]University of Central Florida-US, [2]Princeton University-US, [3]Keele University-UK, [4]University of St. Andrews-UK

ABSTRACT

WASP-43b (Hellier et al., 2011) is the closest-orbiting hot Jupiter (a = 0.0142 AU) with a period of only 0.81 days. However, its host star is the coolest and lowest-mass of any star with a hot-Jupiter (K7V, $M_* = 0.58\ M_\odot$), emitting just enough energy that the planet gets to a modest equilibrium temperature of 1374 K. This configuration led to strong signal-to-noise (S/N) observations and deep eclipses in both Spitzer channels (3.6 and 4.5 μm). Planets with higher S/N ratio allow more accurate measurements of eclipse depths and brightness temperatures and tighter constraints on atmospheric composition and thermal structure. Additionally, we use wavelet denoising to reduce photometric errors further. We present the eclipse depths and brightness temperatures, the possibility of thermal inversion and constraints on molecular abundances and thermal structure. The eclipse timings further refine orbital parameters.

DATA ANALYSIS

Our analysis uses Photometry for Orbits, Eclipses and Transits (POET) to produce light curves from Spitzer Basic Calibrated Frames, fit models to the light curves and assess uncertainties. We start with flagging bad pixels. Then, we reject bad frames, preform denoising, centering and 5x-interpolated aperture photometry (Harrington et al., 2007). To explore the parameter space and estimate uncertainties we apply model fitting routines using a Markov-chain Monte Carlo scheme (MCMC), where systematic corrections and lightcurves are modeled simultaneously (Fig. 1).

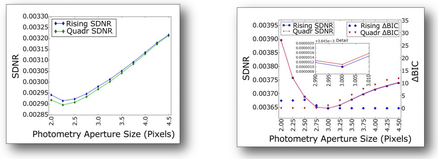

Fig. 2 - Channel 1 and 2 comparison between rising and quadratic ramp models. Plots show SDNR and ΔBIC *vs.* aperture size

The Spitzer IRAC instrument exhibits two well-known systematics. Positional sensitivity ("intrapixel effect", photometry depends on the precise location of the stellar center within a pixel) and time-varying sensitivity ("ramp effect", an increase in flux over time due to charge trapping). For each data set we run all ramp models known in the literature and our position sensitivity technique (see bellow). To determine the best aperture size we search for the solution with the smallest standard deviation of normalized residuals (SDNR, Fig. 2). To choose best model we use Bayesian (BIC) and Akaike information criteria (Campo et al., 2011). Results give eclipse depths, midpoints and estimates for brightness temperature for the best fit models (see tables).

NOVEL TECHNIQUES

BLISS - To model intrapixel effect we use Billinearly-Interpolated Subpixel Sensitivity (BLISS) technique that computes the position-dependent flux at the subpixel level using bilinear and nearest-neighbor interpolation (Stevenson et al., 2011). Using hundreds of control points and optimal bin size we map the pixel surface at high resolution, without a need for any free parameters (Fig. 3 and 4).

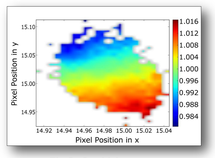

Fig. 3 - Sensitivity map

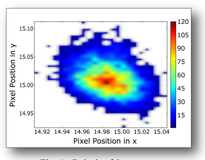

Fig. 4 - Pointing histogram

TIDe - The short exposure time of our observations (2s) allows us to apply our Time-series Image Denoising (TIDe) technique (Stevenson et al., 2012, in preparation). Photon noise, inherent to all astronomical observations is a high-frequency component easily removed with wavelet decomposition, without affecting low-frequency eclipse events. The wavelet-transformation result is a two-dimensional dataset (x-time, y-scale). The lowest level of decomposition describes how the data change on the shortest timescales, thus we can shrink or even eliminate these wavelet coefficients. We test several levels and determine the timescale at which the photon noise has dominant effect (Fig. 5). Image centers, photometric results and position sensitivity map are improved by applying this technique.

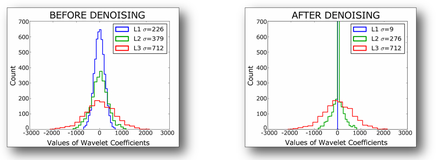

Fig. 5 - L2 level of decomposition histogram at point 15, 15 before and after denoising

ORTHOGONALIZATION - For the most correlated parameters we apply an orthogonalization technique. We first run 10^5 iterations to sample the posterior distribution. Then, we rewrite the ramp model with orthogonalized parameters using a transformation matrix. The orthogonalization shifts the origin of the center of the distribution, divides each parameter by its standard deviation to give a uniform scale in all directions, and rotates the subspace to minimize the correlations (Fig. 6).

LIGHT CURVES

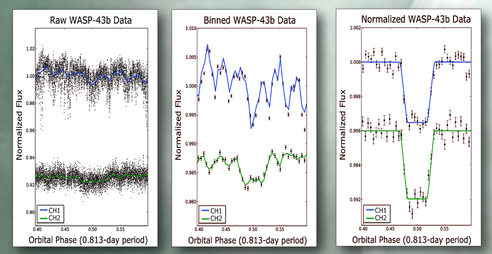

Fig.1 - Raw, binned and systematics-corrected normalized light curves of WASP-43b for channel 1 (3.6 μm) and channel 2 (4.5 μm).

Spitzer channel	Ramp model	Eclipse depth (%)	Brightness T. (K)
3.6 μm	quadratic	0.3520 ± 0.0097	1828
4.5 μm	quadratic	0.4202 ± 0.0122	1703

Spitzer channel	Denoising level	Intrapixel model	Ortho.
3.6 μm	L2	bilinear	yes
4.5 μm	L3	bilinear	yes

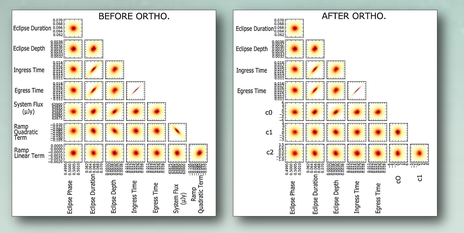

Fig.6 - Parameter correlations for channel 1 before and after orthogonalization. We ortogonalize system flux and both ramp parameters to provide a coordinate system in which MCMC can sample efficiently.

ORBITAL DYNAMICS

The timing of the secondary eclipses suggest a circular orbit. The weighted average eclipse phase of the two eclipses, after an eclipse-transit light-time correction of 14.2 s is 0.50019 ± 0.00020, indicating that $e\cos(\omega) = 0.00031 \pm 0.00031$. This value is less than 0.0009 at 3σ level. The result is consistent with the circular orbit adopted by Hellier et al. (2011).

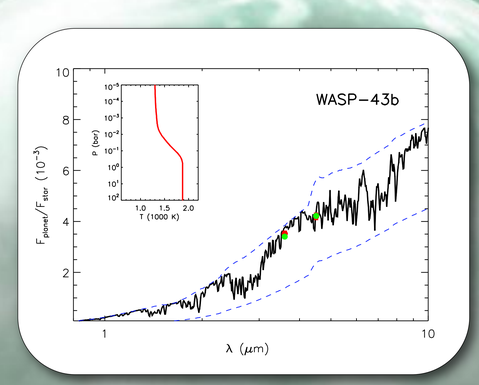

Fig.7 - Observations and model spectra for dayside emission from WASP-43b
The black solid line in the main panel shows a model spectra without a thermal inversion (derived using the method of Madhusudhan and Seager 2009, 2010). The corresponding pressure-temperature profile is shown in the inset. The blue dashed lines are blackbody curves at 1873 K and 1300 K (lowest and highest temperatures in the atmosphere admissible by the data). The green dots are binned model in both Spitzer channels. The red dots show our observations in channel 1 (3.6 μm) and 2 (4.5 μm).

ATMOSPHERE

To constrain molecular composition and discuss the presence of thermal inversion we use the atmospheric temperature and abundance retrieval method derived by Madhusudhan and Seager (2009), (2010). This method incorporates a Bayesian parameter estimation algorithm (Markov-Chain Monte Carlo routine with a Metropolis-Hastings scheme within the Gibbs sampler) for very fine sampling of the parameter space, resulting in posterior probability distributions and goodness-of-fit contours that constrain the model parameters. The Bayesian approach and running millions of models within allowed parameter space tell us what we can say about the atmosphere even with just two data points.

The parameter space of allowed models is constrained based on the data and energy balance at the top of the atmosphere. The pressure-temperature profile captures a signature of temperature inversion and reveals day-night energy distribution.

The data exclude a strong thermal inversion (the brightness temperature in the 3.6-μm is greater that in 4.5-μm channel, Fig. 7). The molecular composition is solar and the day-night redistribution for zero-albedo is ~25%.

WASP-43b has almost the same irradiation as HD 209458b. The lack of a strong thermal inversion in this planet is surprising, since HD 209458b hosts an inversion (e.g., Burrows et al., 2007, Madhusudhan and Seager 2009). This is another example, along with WASP-14b (Blecic et al., 2011), WASP-12b (Madhusudhan et al., 2011), TrES-3b (Fresin et al., 2010, and XO-1b (Machalek and et al., 2009), that contradicts the pM-pL classification scheme by Fortney et al., 2008. On the other hand, Hellier at el., 2011 show the presence of strong Ca H+K emission, which indicates that the WASP-14 star is active. This would explain the lack of an inversion based on Knutson's hypothesis (Knutson et al., 2010).

REFERENCES

Blecic et al., 2011, arXiv:1111.2363v1
Burrows et al., 2007, ApJ, 668, L171
Campo et al., 2011, ApJ, 727, 125
Fortney et al., 2008, ApJ, 678, 1419
Fresin et al., 2010, ApJ, 711, 374
Harrington et al., 2007, Nature, 447, 691
Hellier et al., 2011, arXiv:1104.2823
Knutson et al., 20110 ApJ, 720, 1569K
Machalek et al., 2009, ApJ, 684, 1427
Madhusudhan and Seager 2009, ApJ, 707:24-39
Madhusudhan and Seager 2010, ApJ, 727, 261
Madhusudhan et al., 2011, Nature, 469, 64
Stevenson et al., 2011, arXiv:1108.2057
Stevenson et al., 2012, in preparation

CONTACT

University of Central Florida,
Department of Physics-Planetary Sciences
Orlando, FL 32816-2385

jasmina@physics.ucf.edu